Scientific Research Publishing

World Journal of Engineering and Technology, 2026, 14(2), 454-470
https://www.scirp.org/journal/wjet
ISSN Online: 2331-4249
ISSN Print: 2331-4222

Effects of Injection Timing on Operating Performance of Aero Two-Stroke Piston Engine

Liwen Zhu, Liang Liu, Kaifeng Cao, Yifei Wu*, Jinwu Wu, Xueyun Gao, Chengyu Han

School of Power and Energy, Nanchang Hangkong University, Nanchang, China
Email: *wuyifei.jx@163.com

How to cite this paper: Zhu, L.W., Liu, L., Cao, K.F., Wu, Y.F., Wu, J.W., Gao, X.Y. and Han, C.Y. (2026) Effects of Injection Timing on Operating Performance of Aero Two-Stroke Piston Engine. *World Journal of Engineering and Technology*, **14**, 454-470.
https://doi.org/10.4236/wjet.2026.142026

Received: March 30, 2026
Accepted: May 24, 2026
Published: May 27, 2026

Abstract

According to the relevant technical parameters of the spark-ignition aviation two-stroke gasoline engine, a one-dimensional simulation model of the whole engine was established on the GT-Power software platform. The initial and boundary conditions required for three-dimensional simulation were obtained through the one-dimensional model. On this basis, three-dimensional numerical simulation of the studied aviation two-stroke engine was carried out using Converge software, and the effects of different injection timings on the in-cylinder mixture formation and combustion process were analyzed. The results indicate that a reasonable injection timing can achieve superior in-cylinder mixture uniformity, thereby optimizing the combustion performance of the engine. Overly early injection leads to excessive fuel being directly discharged from the cylinder, while overly late injection results in insufficient uniformity of the in-cylinder mixture, both of which deteriorate the combustion effect. When the engine operates at 5400 r/min, the optimal fuel injection timing is −130˚CA.

Keywords

Spark-Ignition Aviation Two-Stroke Gasoline Engine, Fuel Injection Timing, Combustion, Mixture Formation, Numerical Simulation

1. Introduction

Aviation piston engines are classified into spark-ignition and compression-ignition types in terms of ignition modes. Spark-ignition aviation piston engines present outstanding advantages including high power-to-weight ratio, compact size, simple structure, high thermal efficiency, superior reliability, low cost and low maintenance cost [1] [2], which are widely adopted as the power sources in unmanned aerial vehicle (UAV) engineering [3] [4]. Compared with four-stroke en-

gines, two-stroke engines feature high power density and high rotational speed; hence, two-stroke piston engines dominate the current UAV piston engine application market [5] [6].

In aviation two-stroke reverse scavenging engines, the mixture formation is not only correlated with the in-cylinder flow field but also affected by fuel injection timing [7] [8]. Meanwhile, restricted by the short duration of a single working cycle, two-stroke engines are more sensitive to the variation of fuel injection timing [9]. The uniformity of in-cylinder air-fuel mixture is critical to engine comprehensive performance. Therefore, it is essential to improve the matching degree between fuel injection timing and in-cylinder flow field, so as to optimize the formation and distribution of in-cylinder mixture, refine the combustion process, and further promote the overall performance of the engine.

The comprehensive performance of aviation piston engines covers dynamic performance, emission performance, fuel economy, high-altitude performance and other indicators, which play a decisive role in the design, research, development and optimization of engines [10]. Domestic and international scholars have conducted extensive researches on the influence of fuel injection timing on mixture formation. Li Changsheng [11] adopted AVL Fire software to conduct numerical simulation on the mixture formation and combustion process of the TKD600 engine, and explored the characteristics of mixture formation, as well as the influence laws of fuel injection on fuel wall impingement, mixture formation and ignition energy on combustion performance. The research indicates that different fuel injection parameters exert differentiated effects on in-cylinder air flow motion and fuel atomization. For high-speed diesel engines with small cylinder bore, reasonable injection parameters can accelerate mixture formation and improve combustion quality. Zhu Hongfei [12] experimentally investigated the effects of variable injection timing on in-cylinder spray evolution and combustion characteristics of a single-cylinder four-stroke engine. Nevertheless, researches focusing on the combustion process of two-stroke piston engines under diverse injection timings are still insufficient. Shi Yun [13] studied the mixture formation process of two-stroke heavy-fuel piston engines, and the results verified that the optimization of injection scheme and reasonable organization of in-cylinder flow motion are conducive to the formation of homogeneous in-cylinder mixture. Wang and Hu [14] evaluated the effects of fuel injection timing and ignition strategy on combustion and knocking characteristics of a two-stroke direct-injection spark-ignition (DISI) engine fueled with aviation kerosene.

At present, numerical simulation has become a core method for in-depth engine research, which can simulate the full-scale working process of engines and acquire engine operating characteristics under various working conditions [15] [16]. In this paper, a one-dimensional simulation model of the aviation two-stroke engine is established on the GT-Power platform according to the actual technical parameters under variable injection timing conditions. The initial and boundary conditions required for three-dimensional numerical calculation are obtained via

the one-dimensional model. On this basis, Converge software is applied to carry out three-dimensional numerical simulation of the research object, which can intuitively and accurately characterize the variation of multiple physical fields throughout the engine working cycle.

2. Establishment of Engine Simulation Model

2.1. Establishment of Engine One-Dimensional Simulation Model

The research object of this paper is a two-cylinder horizontally opposed spark-ignition two-stroke piston engine with reed valve intake. Gasoline is selected as the fuel, and its main physicochemical properties are as follows: density of 0.70 - 0.75 kg/L, flash point of −45˚C - −25˚C, freezing point of −80˚C, theoretical air-fuel ratio of 14.8, and lower heating value of 44000 kJ/kg. The main technical parameters are listed in Table 1.

Table 1. Main technical parameters of the engine.

parameters	value
total displacement/ml	119.8
bore/mm	44
stroke/mm	39.4
connecting rod length/mm	70
compression ratio	10.8
Exhaust port opening phase angle/˚CA ATDC	105
Exhaust port closing phase angle/˚CA ATDC	255
Scavenge port opening phase angle/˚CA ATDC	125
Scavenge port closing phase angle/˚CA ATDC	235

The one-dimensional performance simulation calculation of engine is also defined as thermodynamic cycle calculation. To efficiently and accurately reproduce the actual operating conditions of the engine, the whole calculation process is divided into four parts: gas exchange process, heat transfer process, combustion process, and the unsteady gas dynamic process of the intake and exhaust system [17]. The one-dimensional performance simulation model established by GT-Power is shown in Figure 1.

GT-Power possesses quasi-three-dimensional simulation capability for engine calculation. It can not only analyze key performance parameters such as power output, fuel consumption and emission characteristics, but also simulate the variations of pressure, temperature and mass flow along the gas flow path inside the engine. In addition to the simulation of steady-state operating conditions, the software can accurately predict the transient operating processes. Accordingly, reasonable initial and boundary conditions can be provided for the subsequent three-dimensional numerical simulation. Table 2 presents the initial and bound-

ary conditions obtained from one-dimensional simulation under the specified operating conditions: engine speed of 5400 r/min, 100% throttle opening, ignition advance angle of 29˚CA, fuel injection timing of −130˚CA, single-cycle fuel injection quantity of 2.38 mg, and injection duration of 12˚CA.

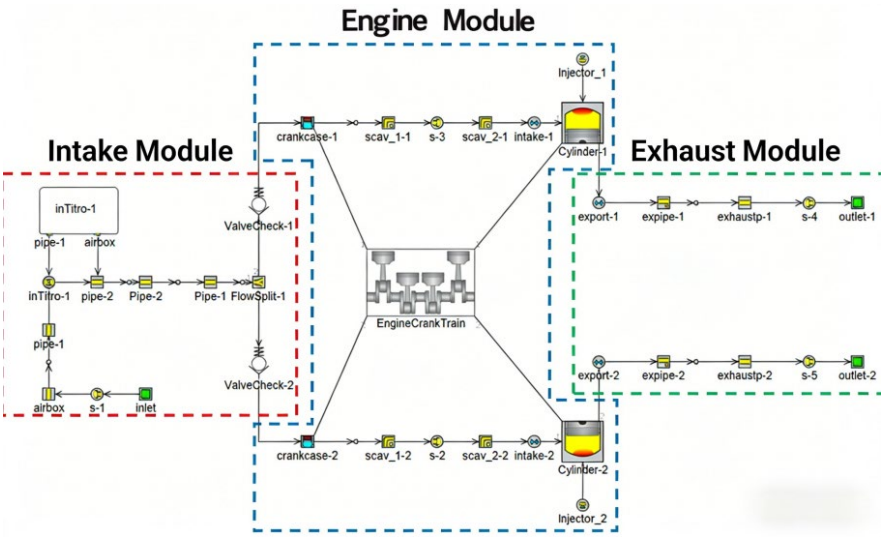

Figure 1. One-dimensional performance simulation model diagram.

Table 2. Initial and boundary conditions for simulation calculation.

parameters	value
Scavenge passage pressure (Pa)	112642.43
Scavenge passage temperature (K)	322.6
In-cylinder pressure (Pa)	320981.1
In-cylinder temperature (K)	1430.9
exhaust passage pressure (Pa)	91192.5
exhaust passage temperature (K)	514.5
Exhaust port pressure at cylinder top (Pa)	91192.5
Exhaust port temperature at cylinder top (K)	514.5
Cylinder head temperature (K)	550
Cylinder wall temperature (K)	400
Piston temperature (K)	550
Scavenge passage wall temperature (K)	322.6
Exhaust passage wall temperature (K)	514.5
Exhaust port wall temperature at cylinder top (K)	514.5
Scavenge passage inlet temperature (K)	322.6
Exhaust passage outlet pressure (Pa)	91192.5
Exhaust passage outlet temperature (K)	514.5
Exhaust port outlet pressure at cylinder top (Pa)	91192.5

2.2. Establishment of Engine Three-Dimensional Simulation Model

In this paper, only a single cylinder is selected as the research object for the three-dimensional simulation, and the crankcase modeling is omitted. Therefore, the established three-dimensional engine simulation model mainly consists of three domains: the scavenge passage, the exhaust passage, and the cylinder with combustion chamber. The adopted physical models are specified as follows: the RNG k-ε model for turbulence, the KH-RT model for droplet breakup, the Wall Film model for droplet impingement, the Frossling model for fuel evaporation, the L-type Energy Source model for ignition, and the SAGE model for combustion. In this study, the SAGE combustion model is adopted to simulate and calculate the in-cylinder combustion process of the engine. The chemical reaction mechanism employs an isooctane mechanism developed by Dalian University of Technology, which contains 41 species and 124 reaction steps [18].

Proposed by Tuns [19], a multi-step chemical reaction mechanism can be expressed in the following form:

$$\sum_{m=1}^{M} V'_{m,r} X_m \Leftrightarrow \sum_{m=1}^{M} V''_{m,r} X_m \quad r = 1, 2, \cdots, R \tag{1}$$

where $V'_{m,r}$ and $V''_{m,r}$ represent the stoichiometric coefficients of reactants and products, respectively. Herein, m denotes the chemical species, r stands for the elementary reaction, R is the total number of reaction steps, and X_m refers to the chemical formula of the species m. The net production rate of each chemical species can be calculated by Equation (1).

$$\dot{\omega}_m = \sum_{r=1}^{R} V_{m,r} q_r \quad m = 1, 2, \cdots, M \tag{2}$$

where $\dot{\omega}_m$ denotes the net production rate, M is the total number of chemical species, and $V_{m,r}$ in the above equation is defined as:

$$V_{m,r} = V''_{m,r} - V'_{m,r} \tag{3}$$

The reaction progress parameter q_r of the r reaction step is expressed by the following equation:

$$q_r = k_{fr} \prod_{m=1}^{M} \left[X_m\right]^{V'_{m,r}} - k_{rr} \prod_{m=1}^{M} \left[X_m\right]^{V''_{m,r}} \tag{4}$$

where $\left[X_m\right]$ is the molar concentration of the species m, k_{fr} and k_{rr} denote the forward r and reverse rate coefficients of the reaction, respec-tively.

For a given computational cell, the governing equations based on mass conservation and energy conservation can be solved.

$$\frac{\mathrm{d}\left[X_m\right]}{\mathrm{d}t} = \dot{\omega}_m \tag{5}$$

$$\frac{\mathrm{d}T}{\mathrm{d}t} = \frac{V\dfrac{\mathrm{d}P}{\mathrm{d}t} - \sum_m \left(\overline{h}_m \dot{\omega}_m\right)}{\sum_m \left(\left[X_m\right] \overline{c}_{p,m}\right)} \tag{6}$$

where V is the volume, T is the temperature, P is the pressure, $\dot{\omega}_m$ repre-

sents the net production rate of species m, and $\overline{h}_m$ and $\overline{c}_{p,m}$ are the molar specific enthalpy and molar constant-pressure specific heat capacity of species m, respectively.

Figure 2 presents the fluid domain of the engine.

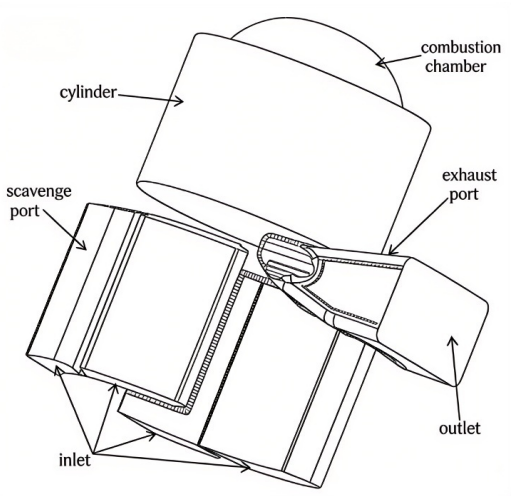

Figure 2. Internal flow field model of the engine.

This paper defines several cross-sections for subsequent cloud contour analysis, as shown in Figure 3. The symmetry planes along the X-axis and Y-axis of the cylinder are defined as the Y-Z cross-section and X-Z cross-section, respectively. The plane 3 mm away from the X-Z cross-section is defined as the X-Z-3 cross-section.

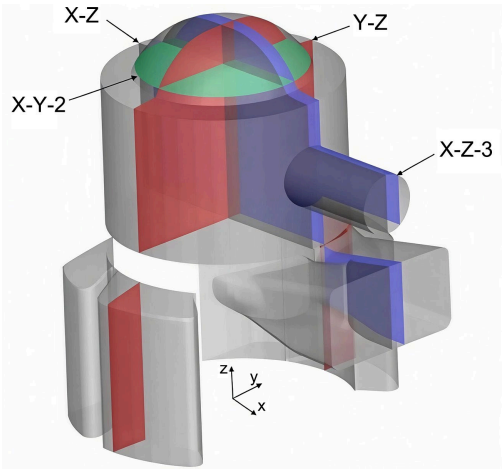

Figure 3. Schematic of the defined cross-sections.

Mesh quality is one of the direct factors affecting the accuracy of numerical simulation results [20]. Converge software provides tools to control mesh size and realize the coarsening or refining of the base mesh. It mainly includes two encryption strategies: fixed embedding, which improves mesh accuracy by fixed refinement at designated positions and moments, and adaptive mesh refinement, which

adjusts mesh size according to flow fluctuation and moving boundary conditions. In engine simulation, the two methods are generally used cooperatively. In this model, two layers of spherical fixed refinement regions with radii of 3 mm and 1 mm are established around the spark plug at the ignition moment, with refinement levels of 2 and 3 respectively. During fuel injection, a conical fixed refinement region is arranged along the fuel spray path with a refinement level of 2. Meanwhile, adaptive mesh refinement is activated with a refinement level of 1. The mesh refinement configuration is shown in Figure 4. Local mesh refinement in key working stages captures critical flow phenomena and effectively improves the accuracy of simulation results.

To ensure the reliability of simulation results, basic grid sizes of 1.4 mm, 1.2 mm, 1.0 mm and 0.8 mm listed in Table 3 are selected for comparative analysis. Figure 5 shows the variation curves of the calculated average in-cylinder pressure of the engine simulation model under different basic mesh sizes. It can be observed that the influence of mesh size on the average in-cylinder pressure gradually decreases as the basic mesh size declines. The average in-cylinder pressure of Case 1 is slightly higher than that of Case 2, while the mesh number of Case 1 is far larger. Considering comprehensively the calculation accuracy and time cost, a basic mesh size of 1 mm is finally determined.

Table 3. Number of meshes used.

Case	Basic Mesh Size/mm	Mesh number
Case 1	0.8	74065-807513
Case 2	1.0	39347-484230
Case 3	1.2	23354-330646
Case 4	1.4	14473-227549

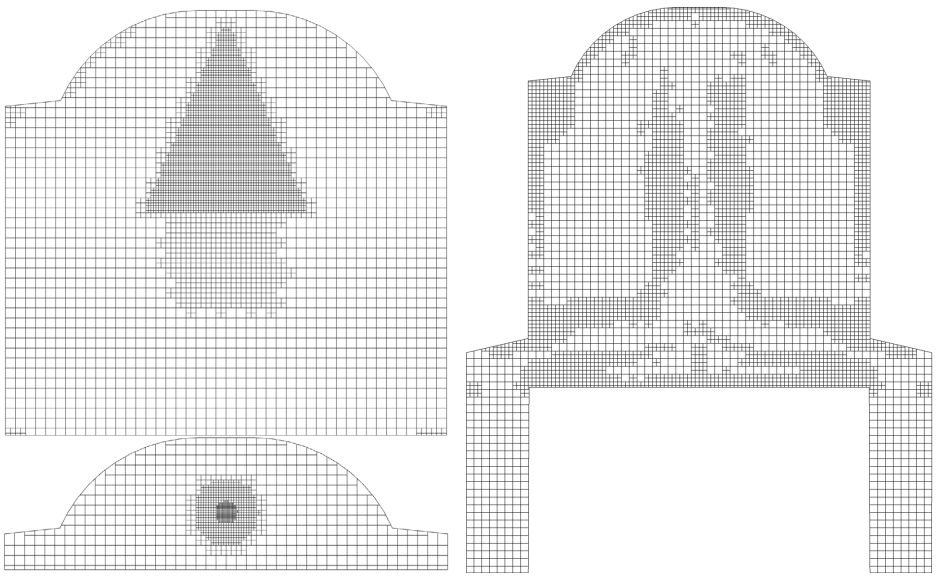

Figure 4. Mesh refinement conditions in the calculation.

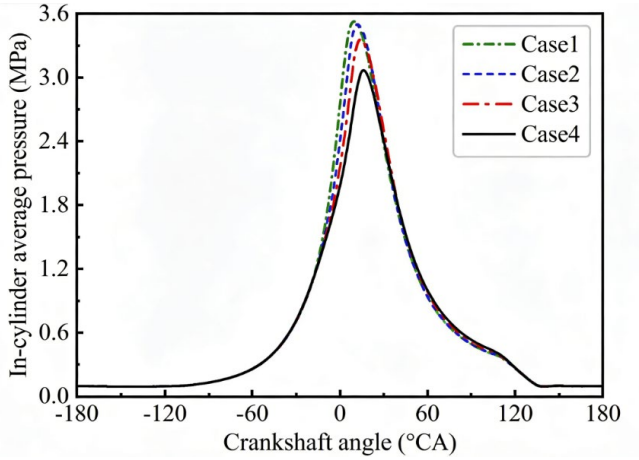

Figure 5. Curves of in-cylinder average pressure variation under different basic mesh dimensions.

Since the crankcase is omitted in the present simulation, the compression process of fresh air inside the crankcase cannot be calculated. However, the pressure in the actual crankcase varies significantly during engine operation, and a constant pressure boundary condition will exert a considerable impact on the simulation accuracy. Therefore, a pressure boundary condition varying with the crank angle must be specified at the inlet of the scavenge passage. This boundary condition was calculated and acquired through one-dimensional simulation, as illustrated in Figure 6.

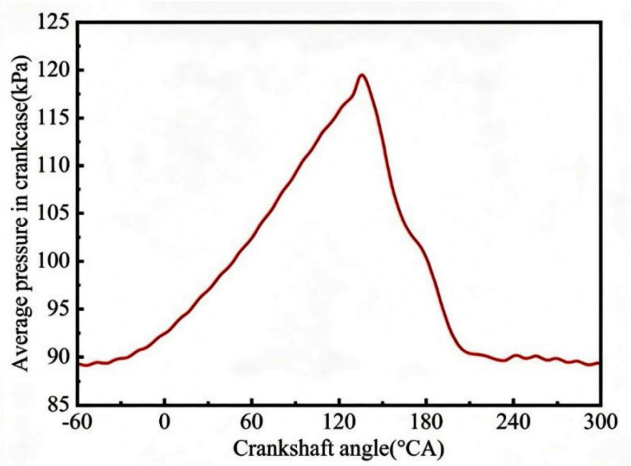

Figure 6. Average pressure variation curve in the crankcase.

3. Study on Mixture Formation and Combustion Process in Engine Cylinder at Different Injection Timings

A proper fuel injection timing enables the engine to obtain a homogeneous air-fuel mixture. Moreover, the aviation two-stroke piston engine studied in this paper has a small displacement, and the time required to complete a single working cycle is short, making the selection of injection timing more stringent. This sec-

tion investigates how injection timing affects the in-cylinder mixture formation and combustion process of the engine, and the relevant operating conditions are presented in Table 4.

Table 4. Engine operating conditions at different fuel injection timings.

Parameters	Value
Engine Speed/r·min^{-1}	5400
Throttle Opening	100%
Scavenge Passage Inclination Angle/˚	13
Ignition Advance Angle/˚CA BTDC	29
Fuel Injection Quantity/mg	2.34
Fuel Injection Timing/˚CA BTDC	120, 125, 130, 135, 140
Injection Duration/˚CA	12

3.1. Analysis of In-Cylinder Fuel Spray

Figure 7 presents the variation of spray penetration distance under different fuel injection timings. The spray penetration distance is defined as the maximum distance between the spray front and the nozzle along the injection direction. The injection timing exerts a significant effect on spray penetration characteristics. An earlier injection timing corresponds to a lower in-cylinder back pressure and a higher peak spray penetration distance. Among all cases, the injection timing of −140˚CA shows the maximum peak penetration distance of 44 mm, leading to the highest risk of fuel wall impingement. By contrast, the timing of −120˚CA has the minimum peak penetration distance of 37 mm, which results in insufficient spray development and a high risk of inadequate mixture formation. Combined with the analysis of spray penetration distance, fuel atomization quality and combustion performance, the injection timing of −130˚CA is determined as the optimal solution. It can effectively avoid fuel wall wetting, ensure sufficient spray development and promote the uniform formation of in-cylinder mixture.

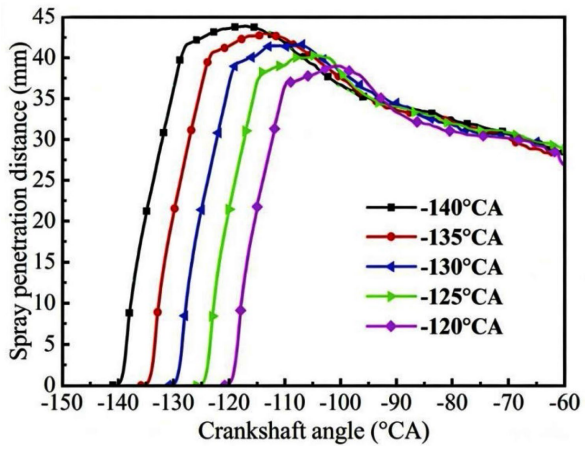

Figure 7. Spray penetration distance variation curves at different fuel injection timings.

The fuel atomization effect during injection is commonly evaluated by the fineness and uniformity of fuel droplets. Finer droplets with a more uniform distribution indicate superior atomization quality. The droplet fineness is generally characterized by the Sauter Mean Diameter (SMD), which is defined as the ratio of the total volume of all droplets to their total surface area. The mathematical expression is as follows:

$$\mathrm{SMD} = \frac{\sum_{i=1}^{N_{tot}} N_i d_i^3}{\sum_{i=1}^{N_{tot}} N_i d_i^2}. \tag{7}$$

In the formula, N_{tot} represents the number of droplet diameter groups; N_i is the total number of droplets with the diameter of d_i; d_i denotes the droplet diameter.

Here is the fully polished, academically standardized English translation, consistent with your previous CFD/two-stroke engine terminology: Figure 8 illustrates the variation of droplet Sauter Mean Diameter (SMD) under different fuel injection timings. It can be seen that the peak SMD values under various injection timings remain approximately 0.20 mm, indicating that the initial droplet size produced during injection is barely affected by injection timing. After the end of injection, secondary breakup and fuel evaporation occur under the influence of in-cylinder airflow, causing a rapid reduction in SMD. A later injection timing corresponds to a lower SMD in the stable stage, presenting a clear regular trend. The −120˚CA case exhibits the smallest stable SMD and the best atomization performance, yet it faces the risk of insufficient mixture preparation. In contrast, the early injection condition of −140˚CA allows fuel to reside in the cylinder for an excessively long period, which aggravates droplet coalescence and wall wetting, consequently increasing droplet size before combustion and deteriorating overall atomization quality. For timings ranging from −125˚CA to −130˚CA, the SMD remains at a moderate level with sufficient evaporation time, achieving a reasonable balance between atomization quality and mixture formation duration. In terms of fuel atomization alone, the late injection strategy at −120˚CA shows distinct advantages. Nevertheless, practical engine calibration requires comprehensive consideration of combustion phasing, power performance, and emission characteristics. By compromising atomization performance and mixture preparation time, the range of −125˚CA to −130˚CA is identified as the optimal injection interval for balancing atomization behavior and combustion efficiency.

3.2. Analysis of In-Cylinder Mixture Formation and Distribution

Figure 9 shows the variation of in-cylinder fuel vapor mass at different fuel injection timings. It can be observed that, during the injection period under all tested timings, the in-cylinder fuel vapor mass rises rapidly at first and then tends to stabilize. The injection timing exerts a significant influence on fuel evaporation characteristics. As the injection timing is delayed, the final stable value of gaseous fuel inside the cylinder increases gradually. The −140˚CA condition presents the

lowest stable vapor mass of 1.98 mg. The value rises to 2.05 mg at −135˚CA and further increases to 2.18 mg at −130˚CA. The stable vapor mass continues to increase slightly at −125˚CA and −120˚CA, reaching 2.28 mg and 2.30 mg, respectively, with only a minor discrepancy between the two cases. An excessively advanced injection timing induces severe fuel wall wetting, which causes a temporary decline in gaseous fuel mass and imposes adverse effects on combustion and emissions. By contrast, the range of −120˚CA to −125˚CA effectively avoids wall wetting caused by overly early injection while maintaining sufficient evaporation duration. This enables the in-cylinder fuel vapor mass to reach a relatively high level by the late compression stroke, thereby forming the optimal injection advance angle range for fuel evaporation performance.

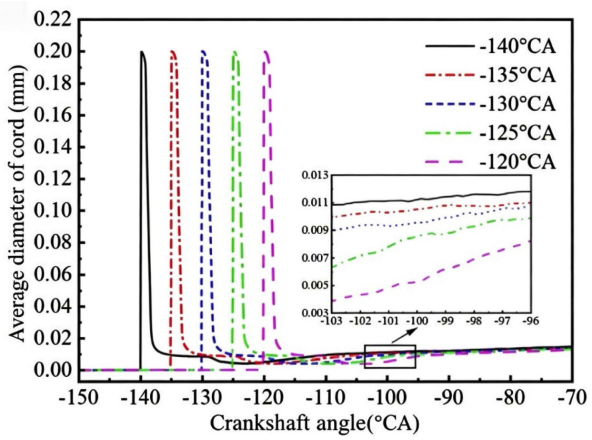

Figure 8. Fuel sauter mean diameter variation curves at different fuel injection timings.

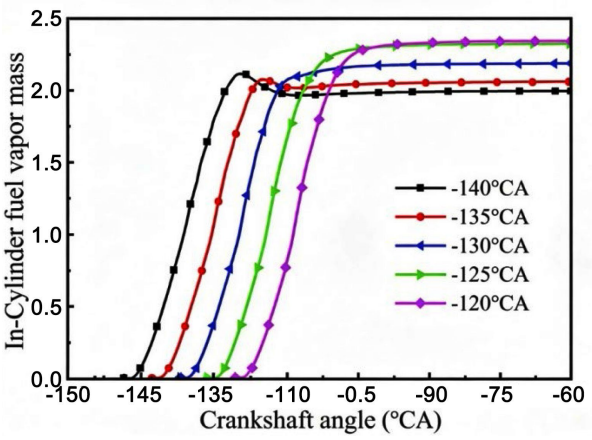

Figure 9. In-cylinder fuel vapor mass variation curves at different fuel injection timings.

Figure 10 presents the in-cylinder equivalence ratio distribution of the mixture at the ignition moment under different fuel injection timings. It can be seen that the mixture distribution is the most uniform at the injection timing of −140˚CA. The advanced injection provides a longer mixing time for fuel and air. Meanwhile, the exhaust port is largely open during injection, and the strong in-cylinder tum-

ble flow facilitates fuel diffusion. Nevertheless, an excessively early injection timing causes a large number of fuel droplets to be directly discharged from the cylinder during injection. Considerable fuel vapor also flows out of the cylinder before the exhaust port closes, resulting in an overall low equivalence ratio of the combustible mixture. As the injection timing is delayed, the equivalence ratio gradually increases in the region near the exhaust port. This indicates that fuel tends to accumulate in this area under retarded injection. The shortened mixing time between fuel and air restricts the diffusion of high-concentration fuel to leaner regions, thereby further raising the local equivalence ratio.

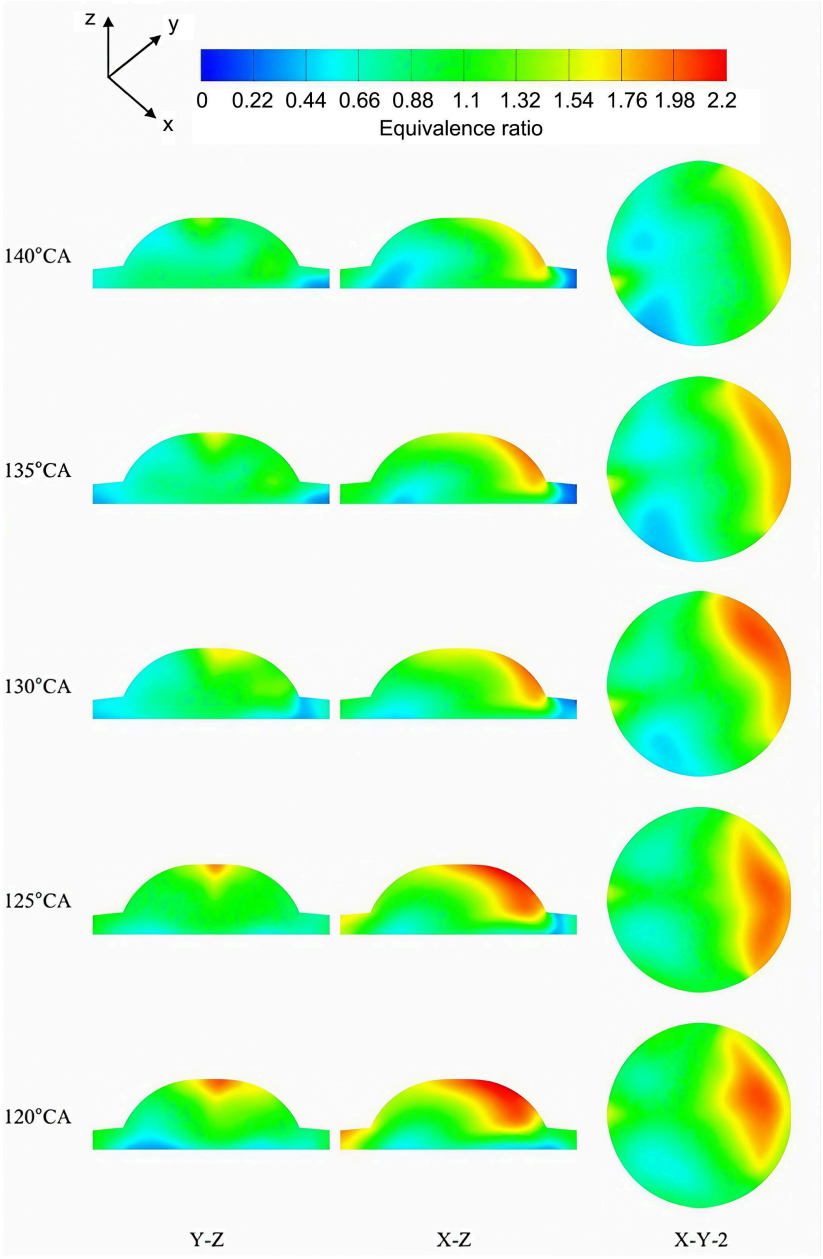

Figure 10. Contour distribution of mixture equivalence ratio at ignition under different fuel injection timings.

Figure 11 shows the equivalence ratio of the mixture near the spark plug at the ignition moment under different fuel injection timings. It is observed that the equivalence ratio around the spark plug gradually increases as the injection timing is retarded.

At the injection timing of −130˚CA, the equivalence ratio near the spark plug reaches 1.05 at ignition, which deviates by only 5% from the stoichiometric value and is conducive to reliable ignition. When the injection timing is delayed to −125˚CA and −120˚CA, the local equivalence ratio rises to 1.20 and 1.28, corresponding to deviations of 20% and 28%, respectively. An over-rich mixture tends to cause incomplete combustion and even ignition failure.

In contrast, with advanced injection timings of −135˚CA and −140˚CA, the equivalence ratio around the spark plug decreases to 0.87 and 0.74, with deviations of 13% and 26%. An overly lean mixture leads to unstable combustion and further induces cycle-to-cycle variation and misfire.

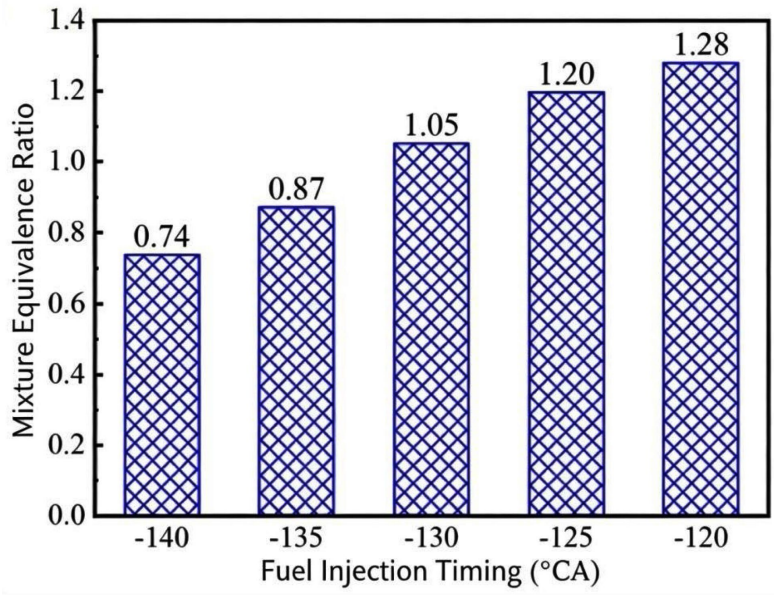

Figure 11. Mixture equivalence ratio at spark plug during ignition under different fuel injection timings.

3.3. Analysis of In-Cylinder Combustion Process

Figure 12(a) illustrates the variation of in-cylinder average pressure at different fuel injection timings. It can be observed that the peak in-cylinder average pressure first increases and then delays with the retardation of injection timing. At the injection timing of −130˚CA, the peak in-cylinder pressure reaches the maximum value of 3.4 MPa, which is significantly higher than 3.1 MPa at −120˚CA. Meanwhile, the peak occurs within a reasonable range of 10˚CA - 15˚CA, indicating a more sufficient combustion process and higher power output capacity. This condition realizes maximum work output and avoids knock and excessive mechanical load caused by an overly rapid pressure rise.

Figure 12(b) presents the variation of in-cylinder average temperature under various injection timings. As the injection timing is retarded, the peak in-cylinder average temperature also rises first and then declines. The maximum peak temperature of 2200 K appears at −130˚CA, with its peak position occurring the earliest. This demonstrates that the fuel combustion is more sufficient under this operating condition, which maximizes the combustion efficiency and efficiently converts combustion heat energy into piston work.

The results reveal that the regulation effect of injection timing on combustion phase directly determines the power performance and thermal efficiency of the engine. Accordingly, −130˚CA is the optimal injection advance angle that balances combustion sufficiency and operational stability under the present condition.

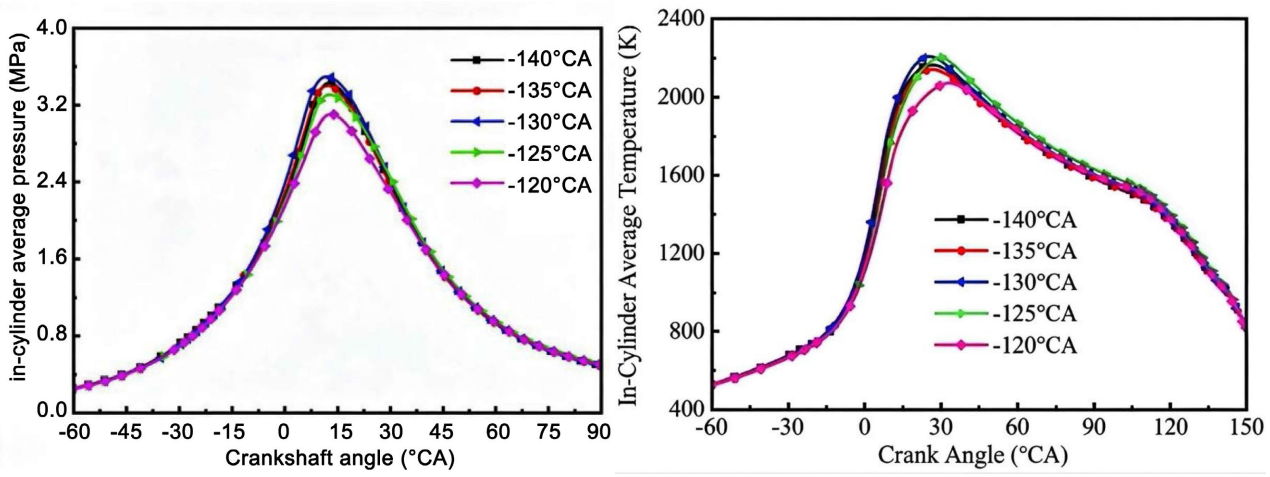

(a) (b)

Figure 12. Variation curves for multiple in-cylinder combustion parameters under different fuel injection timings. (a) In-cylinder average pressure variation curve; (b) In-cylinder average temperature variation curve.

Figure 13 presents the contour nephograms of in-cylinder temperature distribution during the combustion process under different fuel injection timings. As illustrated, the high-temperature region in the cylinder is the smallest at the crank angle of −17˚CA, while nearly the entire in-cylinder area maintains a high and relatively uniform temperature at 33˚CA. As the injection timing is retarded from −140˚CA to −120˚CA, the overall in-cylinder temperature level increases gradually. The high-temperature zone changes from local concentration to uniform distribution across the whole cylinder, and the temperature gradient decreases significantly. This is attributed to the shortened ignition delay and improved fuel-air mixing efficiency under retarded injection, which promotes sufficient combustion reactions and uniform flame propagation. At the injection timing of −130˚CA, an optimal balance between temperature field uniformity and combustion intensity is achieved, yielding high combustion efficiency and providing a direct reference for the optimization of the corresponding fuel injection strategy.

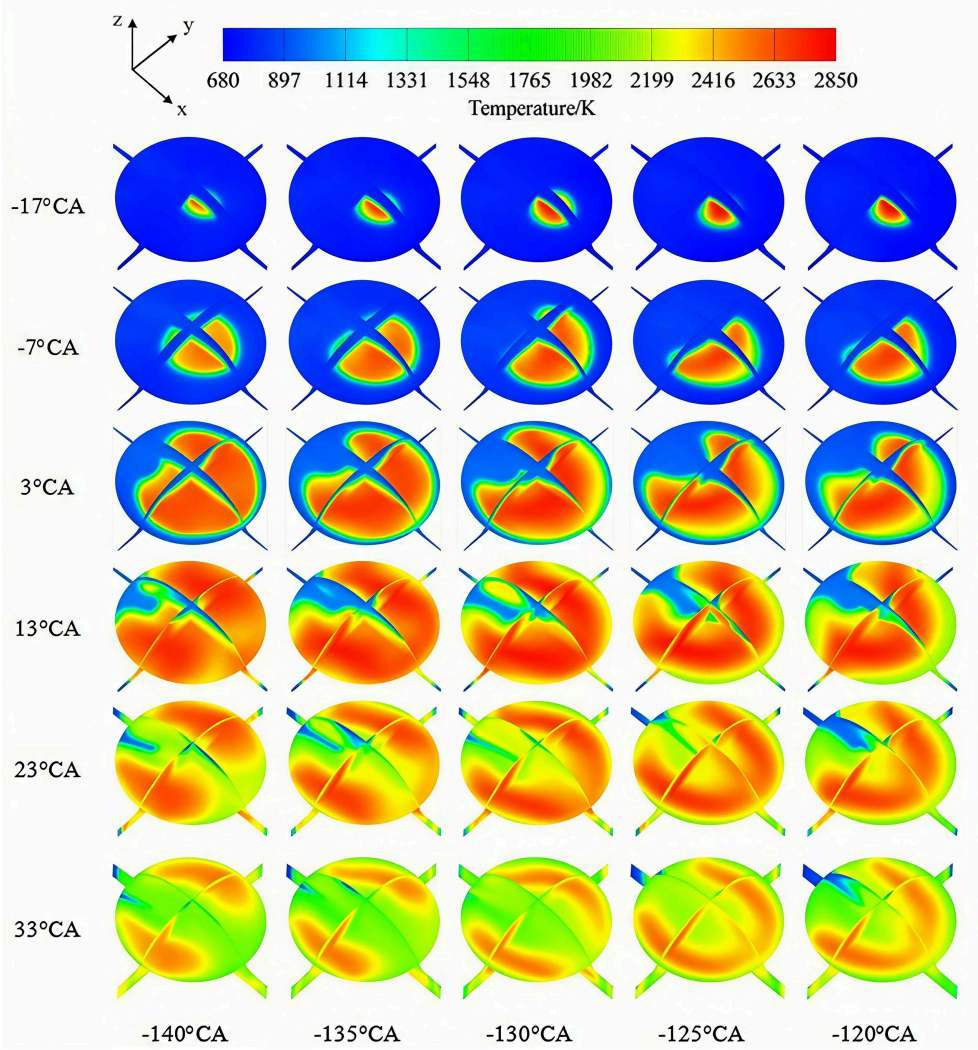

Figure 13. Temperature distribution contours of X-Z, Y-Z and X-Y-2 cross-sections inside cylinder under different fuel injection timings.

4. Conclusions

Based on an aeronautical two-stroke piston engine with a scavenge port inclination angle of 13˚, three-dimensional numerical simulation was conducted to investigate the effects of fuel injection timing on engine operating processes under the rated condition: an engine speed of 5400 r/min, full throttle opening, a single injection quantity of 2.38 mg and an injection duration of 12˚CA. The research results can provide a theoretical reference for the optimization of engine control parameters. The main conclusions are summarized as follows:

1) An advanced injection timing leads to a larger peak spray penetration distance. The maximum penetration distance reaches 44 mm at −140˚CA with the highest risk of fuel wall impingement, while the minimum value of 37 mm occurs at −120˚CA, resulting in insufficient fuel-air mixing. In terms of atomization performance, the initial Sauter Mean Diameter (SMD) remains 0.20 mm for all cases. After injection, the decay rate of SMD increases with retarded injection, whereas

excessive retardation will shorten the mixture preparation time.

2) Retarded injection timing effectively increases the in-cylinder fuel vapor mass. The optimal evaporation performance is obtained within the range of −120˚CA - −125˚CA, and the wall wetting caused by advanced injection is avoided. Early injection contributes to uniform mixture distribution but reduces the overall equivalence ratio. Retarded injection induces local fuel enrichment near the exhaust port. The equivalence ratio near the spark plug rises continuously as the injection timing is delayed. The value at −130˚CA is closest to the stoichiometric condition, which is beneficial to stable ignition.

3) With the retardation of fuel injection timing, the peak values of in-cylinder pressure and temperature both show a trend of rising first and then falling. The maximum peaks of in-cylinder pressure and temperature occur at −130˚CA, presenting sufficient combustion and reasonable combustion phase. This condition not only ensures power output, but also avoids knock and excessive mechanical load. Retarding the injection timing promotes a more uniform distribution of the in-cylinder high-temperature region, reduces the temperature gradient, and improves the fuel-air mixing effect. Comprehensive analysis indicates that −130˚CA is the optimal injection advance angle, which balances combustion intensity and temperature field uniformity and effectively improves combustion efficiency.

Funding

This work was supported by Jiangxi Province Natural Science Foundation (20252BAC240057).

Conflicts of Interest

The authors declare no conflicts of interest regarding the publication of this paper.

References

[1] Zhao, Z., Xiong, J. and Sun, Z. (2026) Research on Optimization of Exhaust Structure and Exhaust Noise Reduction for an Aviation Piston Two-Stroke Engine. *Aerospace Science and Technology*, **168**, Article ID: 110718. https://doi.org/10.1016/j.ast.2025.110718

[2] Savioli, T. (2015) CFD Analysis of 2-Stroke Engines. *Energy Procedia*, **81**, 723-731. https://doi.org/10.1016/j.egypro.2015.12.078

[3] Yu, Y., Wei, M., Jiang, Y., Chen, M. and Wu, Z. (2025) Numerical Study on Cylinder Thermal Load Characteristics of Two-Stroke Engine under High-Altitude Environment. *Small Internal Combustion Engine and Vehicle Technology*, **54**, 1-9. (In Chinese)

[4] Qiao, Y., Duan, X., Huang, K., Song, Y. and Qian, J. (2018) Scavenging Ports' Optimal Design of a Two-Stroke Small Aeroengine Based on the Benson/Bradham Model. *Energies*, **11**, Article No. 2739. https://doi.org/10.3390/en11102739

[5] Zheng, C.K. (2020) Research on Electronic Controlled Fuel Injection System of Two-Stroke Piston Engine for Unmanned Aerial Vehicle. Master's Thesis, Xiamen University. (In Chinese)

[6] Li, Y., Wu, H., Liu, Y., Zhang, L., Qiang, Y., Liu, W., *et al.* (2022) Study on Engine

Performance and Combustion System Optimization of a Poppet-Valve Two-Stroke Diesel Engine. *Energies*, **15**, Article No. 3685. https://doi.org/10.3390/en15103685

[7] Zhang, N. (2022) Influence of Injection Timing on Mixture Formation of Two-Stroke Aero-Engine. *Internal Combustion Engine & Parts*, No. 23, 24-26. (In Chinese)

[8] Grabowski, Ł., Pietrykowski, K. and Karpiński, P. (2019) The Zero-Dimensional Model of the Scavenging Process in the Opposed-Piston Two-Stroke Aircraft Diesel Engine. *Propulsion and Power Research*, **8**, 300-309. https://doi.org/10.1016/j.jppr.2019.11.003

[9] Mitianiec, W. (2003) Formation of Fuel Mixture in a SI Two Stroke Engine with Direct Pneumatic Injection. SAE Technical Paper 2003-01-3164.

[10] Liu, Y. (2021) Research on Numerical Simulation Method for Combustion Process of Small Heavy-Fuel Piston Engine. Master's Thesis, Nanjing University of Aeronautics and Astronautics. (In Chinese)

[11] Li, C. (2014) Study on Mixture Formation and Combustion Characteristics of Small High-Speed Aviation Heavy-Fuel Piston Engine. Master's Thesis, Beijing Jiaotong University. (In Chinese)

[12] Zhu, H., Zhang, S., Jiang, X., Du, J., Chen, H. and Li, Y. (2020) Visualization Research on Engine Spray and Combustion under Injection Strategy. *Automobile Applied Technology*, No. 12, 162-165. (In Chinese)

[13] Shi, Y. (2012) Simulation Study on Mixture Formation of Small Spark-Ignition Two-Stroke Piston Heavy-Fuel Engine. Beijing Jiaotong University.

[14] Wang, H., Yang, Y., Zhang, L., Chen, Y., Zhou, Y., Zheng, Z., *et al.* (2022) Numerical Investigation on Combustion System Optimization for Direct Injection of Aviation Kerosene in a Two-Stroke SI Engine for Unmanned Aerial Vehicle. *Fuel*, **329**, Article ID: 125452. https://doi.org/10.1016/j.fuel.2022.125452

[15] Sigurdsson, E., Ingvorsen, K.M., Jensen, M.V., Mayer, S., Matlok, S. and Walther, J.H. (2014) Numerical Analysis of the Scavenge Flow and Convective Heat Transfer in Large Two-Stroke Marine Diesel Engines. *Applied Energy*, **123**, 37-46. https://doi.org/10.1016/j.apenergy.2014.02.036

[16] Krishna, A.S., Mallikarjuna, J.M. and Kumar, D. (2016) Effect of Engine Parameters on In-Cylinder Flows in a Two-Stroke Gasoline Direct Injection Engine. *Applied Energy*, **176**, 282-294. https://doi.org/10.1016/j.apenergy.2016.05.067

[17] Chen, M., Ding, N. and Zhang, X. (2016) Simulation of Automotive Internal Combustion Engine. 5th Edition, China Communications Press Co., Ltd., 79-81. (In Chinese)

[18] Liu, Y., Jia, M., Xie, M. and Pang, B. (2012) Enhancement on a Skeletal Kinetic Model for Primary Reference Fuel Oxidation by Using a Semidecoupling Methodology. *Energy & Fuels*, **26**, 7069-7083. https://doi.org/10.1021/ef301242b

[19] Turns, S.R. (1996) Introduction to Combustion. McGraw-Hill Companies.

[20] Tan, Y., Cao, B., Li, S., *et al.* (2024) Simulation Study on Reverse Scavenging of Two-Stroke Free Piston Engine. *Small Internal Combustion Engine and Vehicle Technology*, **53**, 1-5+38. (In Chinese)